Simulation of Manufacturing Variations in a Z-axis CMOS-MEMS Gyroscope

Sitaraman Iyer and Tamal Mukherjee
Department of Electrical and Computer Engineering,
Carnegie Mellon University, Pittsburgh, PA 15213
(Email: {sita, tamal}@ece.cmu.edu)

ABSTRACT

This paper uses MEMS circuit-level simulation to correlate gyro performance measures such as zero rate output (ZRO), linear acceleration sensitivity (S_a) and cross-axis sensitivity (S_{ca}) to geometrical asymmetries. Elastic and electrostatic asymmetries in the gyroscope may arise due to device-level manufacturing variations in beam width, comb gap and metal mask misalignment in the CMOS-MEMS process. Analytical equations for the non-idealities are derived and compared with the simulation results. The analyses and simulations are used to develop pointers for robust design as well as manufacturing tolerances for limiting non-idealities.

Keywords: manufacturing variations, CMOS-MEMS, gyroscope

1 INTRODUCTION

Vibratory rate microgyroscopes commonly rely on sensing Coriolis-force-induced angstrom-scale vibrations, and are highly sensitive to spurious oscillations arising from geometric imperfections. Though it is commonly acknowledged [1] that the coupling of the drive motion to the sense mode needs to be as small as a few ppm, there is no comprehensive study in public literature of drive motion coupling, external accelerations and cross-axis rotations. Quadrature error arising from elastic cross-coupling has been considered in a few studies. However, in-phase coupling may also arise in gyroscope designs with intentionally mismatched drive and sense modes. Furthermore, robust design techniques to reject width variations across different chips [2] cannot compensate for width mismatch within a device.

Analog designers using digital processes rely on commonly accepted numbers for transistor mismatch [3]. However, MEMS designers lack similar published data on variations. Through simulations and analyses, we aim to establish the need for systematic study of mismatch in MEMS gyroscopes, which are arguably more demanding on the manufacturing process than accelerometers.

In this paper we focus on variations in beam width and comb gap across the gyroscope and metal mask misalignment effects. The gyroscope parameters being studied are Zero Rate Output (ZRO), acceleration sensitivity (S_a) and cross-axis sensitivity (S_{ca}).

2 BACKGROUND

The gyroscope being analyzed (Figure 1) is fabricated in the CMOS-MEMS process [4]. The gyroscope consists of two nested resonators [5]. The outer resonator is suspended by four springs which are relatively rigid along the sensing direction (*x*) and compliant along the driven direction (*y*). The outer resonator is driven at resonance (at frequency ω_{oy}, displacement y_D) and the inner resonator is forced to move along with the outer resonator because the springs suspending the inner resonator are relatively rigid in *y* and compliant in *x*. In the presence of an angular rate Ω_z about the out-of-plane axis, both the resonators experience the Coriolis force in *x*, however, the inner resonator has a larger displacement. The sensing mode resonant frequency (ω_{ix}) is designed to be larger than ω_{oy}. The relative displacement between the two resonators (x_C) is sensed capacitively using differential combs.

$$x_C \approx \frac{2\omega_{oy} y_D \Omega_z}{\omega_{ix}^2 - \omega_{oy}^2} \quad \text{and} \quad \frac{V}{V_m} \approx \frac{4N_s \varepsilon t o_{lps}}{C_T g_s^2} x_C \tag{1}$$

where, N_s, o_{lps}, g_s and t are, respectively, the number of fingers, the lateral overlap, the gap and the vertical overlap of the sensing comb fingers and C_T is the sum of the comb and parasitic capacitances at each sensing node. Setting $\Omega_z = 1°/s$ yields x_C for unit rotation rate.

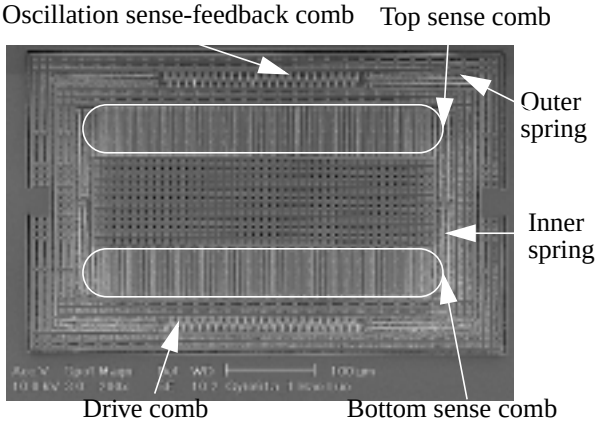

FIGURE 1. SEM of the CMOS-MEMS vibratory z-axis rate gyroscope [5].

An equivalent stiffness matrix is assumed for each spring and the overall system stiffness is obtained by summation of the individual matrices. When the four springs in either the inner or the outer resonator are perfectly matched, the off-diagonal terms in the overall stiffness matrix are zero. However, width mismatch causes non-zero off-diagonal terms resulting in elastic cross-coupling between the drive and the sense modes [6]. For nested resonator gyros, unlike single proof-mass gyros, the elastically coupled displacements and the Coriolis force-induced displacement are not in complete quadrature and therefore, contribute to ZRO and S_a. Spring stiffnesses are denoted as k_{yyo}, k_{xxi} etc. where the subscripts 'o' and 'i' refer to the outer and inner springs respectively.

In the following sections, analyses of ZRO, S_a and S_{ca} are presented. Behavioral simulation is performed using NODAS [7], a library of parameterized *beam*, *plate*, *comb* elements. Layout extraction is used to automatically obtain the gyroscope schematic [8].

3 ZERO RATE OUTPUT

3.1 Beam width variation

There are two sets of four springs as shown in Figure 2. Mismatch within a set of four springs leads to anisoelasticity and therefore, coupling across orthogonal directions.

Coupling of the drive into the sense mode due to relative beam width mismatch (Δ) in outer and inner springs (Figure 2) are respectively given as:

$$\frac{x_{so}}{y_D} = \frac{(\Sigma k_{x\phi zo})(\Sigma k_{y\phi zo})}{(\Sigma k_{xxo})(\Sigma k_{\phi z\phi zo})}\Gamma\left(\frac{\omega_{ix}}{\omega_{oy}}\right) \approx \frac{9L_x k_{yyo}}{16L_y k_{xxo}}\Gamma\left(\frac{\omega_{ix}}{\omega_{oy}}\right)\Delta^2 \quad (2)$$

$$\frac{x_{si}}{y_D} = \frac{\Sigma k_{xyi}}{\Sigma k_{xxi}}\left(\frac{\omega_{oy}}{\omega_{iy}}\right)^2 = \frac{3k_{xyi}}{4k_{xxi}}\left(\frac{\omega_{oy}}{\omega_{iy}}\right)^2\Delta \quad (3)$$

ω_{oy} and ω_{iy} being the resonant frequencies of the outer and inner resonators in the drive (y) direction and

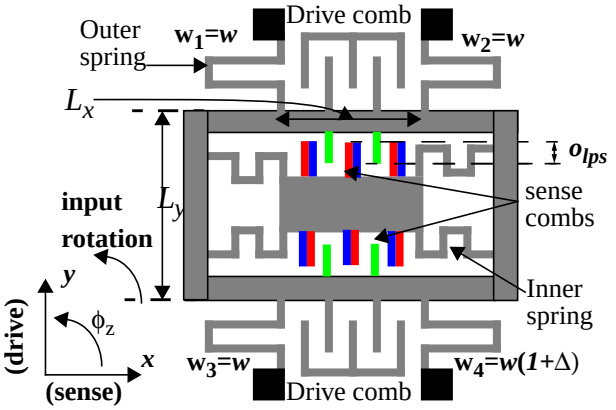

FIGURE 2. Example case for beam width variation and equation for coupling, $w_1 = w_2 = w_3 \neq w_4$.

$\Gamma(a) = 1/(a^2 - 1)$. The outer springs being inherently symmetric, the coupling from drive to sense mode is proportional to Δ^2, whereas, in the asymmetric inner springs the coupling is not only proportional to Δ but is also more than 10 times higher. Also, the gyro topology lends itself to isolating the drive and sense modes i.e., $k_{yyo}/k_{xxo} \ll 1$ and $k_{yyi}/k_{xxi} \gg 1$.

Design options to reduce ZRO include use of wider beam widths to average out lithographic variations, use of symmetric springs and springs which have lower k_{yy}/k_{xx}.

3.2 Comb gap variation

There is no ZRO produced by mismatch of the drive gaps or the sense gaps, unless there is a offset in the comb position. A lateral offset can be produced by a linear acceleration and therefore the analysis of this case is deferred to the discussion of linear acceleration sensitivity.

3.3 Mask misalignment

Mask misalignment causes: lateral curling and mode coupling between the in-plane (x, y) and out-of-plane modes (z). Vertical motion sensitivity of the sense combs is directly proportional to the offset due to lateral curling. Using a parallel plate approximation for the sense comb capacitance, the coupled motion and the ZRO are given by:

$$\frac{z_s}{y_D} = \frac{\Sigma k_{yzo}}{\Sigma k_{zzo}}\left(\frac{\omega_{oy}^2}{\omega_{iz}^2}\right) \text{ and } ZRO = \frac{z_s x_{Os}}{t x_C} \quad (4)$$

where, z_s is the relative vertical motion in the sense comb, t is the nominal vertical overlap, x_{Os} is the position offset.

4 ACCELERATION SENSITIVITY

We limit our discussion below to sensitivity to acceleration in the sensing direction only. Unlike ZRO which can arise due to completely linear coupling, acceleration sensitivity requires a nonlinear "mixer" to multiply two frequency components: the drive frequency (typically a few kHz) and the acceleration component at DC/low frequencies (upto 1 kHz). The drive and sense combs are the main source of nonlinearity being considered here. The voltage output of the differential sense combs can be written as:

$$\frac{V}{V_m} = \frac{4N_s \varepsilon t o_{lps}}{g_s C_T}\left(\frac{x}{g_s} + \left(\frac{x}{g_s}\right)^3 + \left(\frac{x}{g_s}\right)^5 + \ldots\right) \quad (5)$$

where, $x = x_{Os} + x_{As} + x_{Ds}$, is the total displacement of the comb in the sense direction, comprised of a DC offset term, x_{Os}, a sinusoidal acceleration term x_{As} and a drive fre-

quency term x_{Ds} due to coupling. The cubic term in (5) leads to mixing of the three components.

4.1 Beam width variation

Drive motion coupling onto the sense combs is described by (2), (3). Comparing (5) with (1) we get two components: the acceleration sensitivity and the acceleration-squared sensitivity given by:

$$\frac{S_{ax}}{S} = \frac{6x_{Os}x_{As}x_{Ds}}{x_C g_s^2} \text{ and } \frac{S_{a2x}}{S} = \frac{3x_{As}^2 x_{Ds}}{x_C g_s^2} \quad (6)$$

where, S is the gyro sensitivity. x_D in the above equations can arise due to width mismatch in the outer or the inner springs. The S_{a2} term is usually not very significant because $x_{As} \ll x_{Os}$. However, S_{ax} and S_{a2x} being strong functions of the sense comb gap, they effectively constrain the smallest gap that can be used by designers. Also, $x_{As} \propto (1/\omega_{ix}^2)$ implies $S_{a2x}/S \propto 1/\omega_{ix}^2$, where ω_{ix} is the sense mode resonant frequency. A lower bound on ω_{ix} limits the overall sensitivity of the gyroscope. Maximizing sensitivity is vital to the gyroscope performance, particularly in circuit-noise limited systems.

4.2 Comb gap variation

We consider two separate cases for drive comb mismatch and sense comb mismatch.

Relative mismatch Δ in the drive comb gaps, g_d between the top and the bottom combs, causes a force in *x*:

$$F_x = \frac{N_d \varepsilon t}{2} \frac{4x_{Ad}}{g_d^3} (3\Delta) \left(2o_{lpd} V_{dc} V_{ac} + y_D \left(V_{dc}^2 + \frac{V_{ac}^2}{2} \right) \right) \quad (7)$$

where x_{Ad} is the offset in the drive comb due to acceleration in *x* and V_{dc}, V_{ac} are the drive voltages applied. The outer springs are stiff in the x direction, and therefore, lead to small x_{Ad} and an even smaller response to the above force. Therefore, we do not elaborate on this effect.

Mismatched gaps in the two sensing combs (Δ being the relative mismatch), cause a gyro response to acceleration in the sense direction. Using (1) and (3):

$$\frac{V_{ax}}{V_m} = \frac{4N_s \varepsilon t y_s x_{As}}{g_s^2 C_T} \Delta \text{ and } \frac{S_{ax}}{S} = \left(\frac{x_{As} y_D \Delta}{x_C o_{lps}} \right) \left(\frac{\omega_{oy}}{\omega_{iy}} \right)^2 \quad (8)$$

This effect can be reduced by increasing the mode-separation, ω_{iy}/ω_{oy}, or the overlap length, o_{lps}. If one side of the sense combs were anchored to the ground instead of being attached to the outer resonator, then y_s in (8) will be equal to the drive amplitude y_D and as a result the acceleration sensitivity would be much higher. This fact underscores the need for decoupling the drive oscillations from the sense combs. The decoupling is facilitated by the availability of multiple conductors in the CMOS-MEMS process.

4.3 Mask misalignment

Coupling of drive motion to the *z* direction due to metal mask misalignment leads to acceleration sensitivity given as: $S_{ax}/S = (z_s x_{As})/(t x_C)$

5 CROSS-AXIS SENSITIVITY

Beam width and comb gap variations primarily result in in-plane elastic coupling and forces or motion sensitivities. Sensitivity to rotation about the drive (*y*) or the sense (*x*) directions necessarily involves either out-of-plane elastic or electrostatic coupling or comb sensitivity to out-of-plane motion. Therefore, in the discussion below, beam width and comb gap variations are not being considered.

5.1 Rotation about sense direction (Ω_x)

The Coriolis force in z produced for Ω_x is equal to the force produced in x due to Ω_z. However, since the aspect ratio of the spring beams is about 2.5, the *z* resonant mode is higher than the *x* resonant mode leading to reduced Coriolis-force induced displacement. Further, the sense combs are insensitive to vibrations in *z* unless there is a position offset in *x*. The resultant output is given as:

$$\frac{S_{cax}}{S} = \frac{z x_{Os}}{t x_C} = \frac{x_{Os}}{t} \left(\frac{\omega_{ix}}{\omega_{iz}} \right)^2 \quad (9)$$

5.2 Rotation about drive direction (Ω_y)

If the drive motion is coupled to the *z* direction due to mask misalignment, Ω_y leads to a Coriolis force in *x*, the sense direction. In this case the normalized sensitivity is obtained directly as a ratio of the displacements in the *z* and the *y* directions.

$$\frac{S_{cay}}{S} = \frac{z_D}{y_D} = \frac{\Sigma k_{yzo}}{\Sigma k_{zzo}} \quad (10)$$

6 SIMULATION RESULTS

The nominal gyro design uses 1.8 μm beam widths and comb gaps. The analysis for S_{ax} and S_{a2x} suggests that

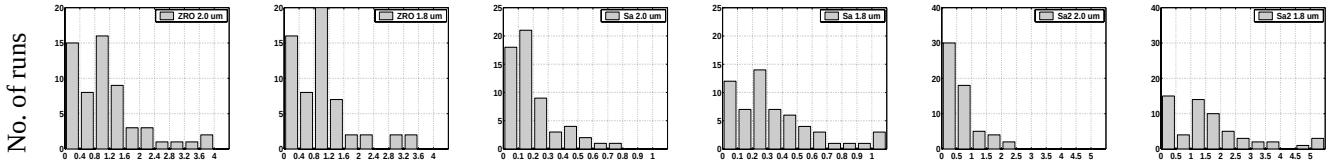

(a) ZRO (X 1000 ˚/s) (b) S_a/S (˚/s/g) (c) S_{a2}/S (X 0.001 ˚/s/g^2)

FIGURE 3. Histograms for widths and gaps = 1.8 μm and 2.0 μm from Monte-Carlo simulation. The significance of the third bin arises due to the variance among the springs leading to a partially Chi-squared like distribution.

larger gaps and larger sense mode resonant frequency will lead to lower acceleration sensitivity. Monte-Carlo simulations were done using nominal beam widths and gaps of 1.8 μm and 2.0 μm. In each case, beam widths in the eight springs and the gaps in the four combs are assumed to be independent, normally distributed random variables (N(w, σ)) with common mean w, equal to the layout dimension (1.8 or 2.0 μm), and standard deviation σ (3σ = 0.05 μm). Each Monte-Carlo analysis involves 60 transient analysis, with the 12 randomly generated dimensions ~ N(w, σ).

The ZRO, S_{ax} and S_{a2x} for the 1.8 and 2.0 μm designs are shown in Figure 3. Since the main contribution to ZRO is most likely the asymmetric topology of the inner springs, it is not affected by larger width and gap. This trend is also predicted by the analytical equations. For equal drive displacements, the nominal gyro sensitivity S for the 2.0 μm design is smaller by about 35%. However, both S_{ax}/S and S_{a2x}/S have reduced significantly, as expected. The mean and standard deviation of S_{ax}/S reduce by about 45% from 0.35 (˚/s)/g to 0.19 (˚/s)/g and from 0.28 (˚/s)/g to 0.16 (˚/s)/g respectively. The absolute reduction in S_{ax} is greater than 60%. Simulations with symmetric inner springs resulted in ZRO reduction of about 90% and greatly reduced offsets due to lateral curling. The simulation values for cross-axis sensitivities are about 100 times smaller than the gyro sensitivity. Increased width and gaps do not have significant impact on cross-axis sensitivity because, the cross-axis sensitivity is mainly dependent on out-of-plane resonant modes and comb sensitivities.

7 CONCLUSIONS

From the analysis and the simulations presented in the preceding sections we arrive at the following conclusions for the ZRO and S_a:

Zero Rate Output:

1. Use symmetric springs only
2. Choose spring topology and position the springs to minimize elastic coupling

Acceleration Sensitivity:

1. Larger comb gaps are better
2. Higher sense mode resonant frequency and larger gaps are better for reduced acceleration-squared sensitivity,

Both the above approaches lead to reduced sensitivity. However, the acceleration rejection obtained is greater than the sensitivity loss. Further, analysis suggests that decoupling of drive vibration from sense combs can reduce linear acceleration sensitivity significantly and potentially eliminate the need for dual anti-phase gyroscopes. Cross-axis sensitivities are found to be about 100 times smaller than the gyro sensitivity and are not strongly dependent on the beam widths and the gaps unlike the acceleration sensitivity. In summary, this methodology allows numerical trade-offs between nominal performance and the ability to reject non-ideal variations.

ACKNOWLEDGEMENTS

This research effort is sponsored by the MARCO Center for Circuits, Systems and Software, the Defence Advanced Research Projects Agency (DARPA) and U. S. Air Force Research Laboratory, under agreement number and F30602-99-2-0545 and in part by the National Science Foundation award CCR-9901171.

REFERENCES

[1] J. A. Geen, “A Path to Low Cost Gyroscopy,” Solid-State Sens. and Act., 51-54, Hilton Head, June 8-11, 1998

[2] C. Acar et al., “A Design Approach for Robustness Improvement of Rate Gyroscopes,” *Modeling and Simulation of Microsystems*, 80-83, Hilton Head, Mar 19-21, 2001

[3] M. J. M. Pelgrom, H. P. Tuinhout, and M. Vertregt, “Transistor Matching in Analog CMOS Applications,” *Int. Elec. Dev. Mtg.*, 915-918, 1998

[4] G. K. Fedder et al., “Laminated High-Aspect-Ratio Microstructures in a Conventional CMOS Process”, *Sensors and Actuators A*, vol. A57, no. 2, pp. 103-110, 1996

[5] H. Luo, G. K. Fedder, L. R. Carley, “An Elastically Gimbaled Z-Axis CMOS-MEMS Gyroscope,” *Int. Sym. Smart Structures & Microsystems*, Hong Kong, Oct. 19-21, 2000

[6] S. Iyer et al., “Analytical Modeling of Cross-axis Coupling in Micromechanical Springs,” *Modeling and Simulation of Microsystems*, 632-635, Puerto Rico, April 19-21, 1999

[7] G. K. Fedder, Q. Jing, “A Hierarchical Circuit-level Design Methodology for Microelectromechanical Systems”, *IEEE Trans. Circ. and Sys II*, vol. 46, no. 10, pp 1309-1315, 1999

[8] B. Baidya et al., “Layout Extraction for Integrated Electronics and MEMS Devices”, *Transducers ‘01 Eurosensors XV*, 280-283, Munich, Germany, June 10-14, 2001